IEEE Access
Multidisciplinary | Rapid Review | Open Access Journal

Received 12 October 2023, accepted 8 November 2023, date of publication 13 November 2023,
date of current version 16 November 2023.

Digital Object Identifier 10.1109/ACCESS.2023.3332245

RESEARCH ARTICLE

An Improved Artificial Neural Network-Based Approach for Total Harmonic Distortion Reduction in Cascaded H-Bridge Multilevel Inverters

YAZEED YASIN GHADI[1], MUHAMMAD SAJID IQBAL[2], MUHAMMAD ADNAN[2], KASHIF AMJAD[2], IJAZ AHMAD[2], AND UMER FAROOQ[3]

[1]Department of Software Engineering, Al Ain University, Al Ain, United Arab Emirates
[2]Department of Electrical Engineering, National University of Computer and Emerging Sciences (FAST), Chiniot-Faisalabad Campus, Chiniot, Punjab 35400, Pakistan
[3]Department of Electrical Engineering, Information Technology University, Lahore 54600, Pakistan

Corresponding author: Muhammad Adnan (m.adnan@nu.edu.pk)

This work was supported by the Faculty Research Support Program of FAST National University of Computer and Emerging Sciences, Pakistan, under Grant FRSG-2023.

ABSTRACT The concept of smart grids has enabled the addition of renewable energy resources in the utility grids. This integration is possible after energy conversion and energy conversion causes the degradation in the quality of electric power. The power quality can be enhanced by reducing the total harmonic distortion (THD) in energy conversion. In this paper, we have presented an improved artificial neural network (ANN) based approach that can be useful to reduce the THD levels in a cascaded H-bridge (CHB) multilevel inverter (MLI). The proposed ANN architecture consists of only one hidden layer with ten neurons and can generate accurate results in both overfitting and underfitting conditions. Due to a smaller number of neurons, the proposed architecture is less complex and can produce results relatively faster as compared to other ANN architectures available in the literature. The proposed ANN architecture is tested on an asymmetrical CHB MLI, and the results are compared with the recent state-of-the-art (SOTA) techniques. The CHB MLI under test had three DC voltage sources with 1:2:4 and inductive loads. The simulations are performed in MATLAB and Simulink environment and the switching angles are optimized by using the ANN architecture. The results have shown a 71.95% improvement in current THDs and a 13.91% improvement in voltage THDs as compared to the SOTA technique. The proposed configuration is 89.6% efficient on inductive load and uses a smaller number of switches. Finally, an experimental setup is created, and the simulation results are validated through various experiments.

INDEX TERMS Artificial neural networks, cascaded H-bridge, multi-level inverter, solar PV system, switching angles, total harmonic distortion (THD).

I. INTRODUCTION

The massive expansion in the global population has exacerbated the use of hydrocarbon-based fuels, which not only contribute to global warming and CO_2 emissions, and put a negative impact on the environment but it is also proved to be one of the most susceptible nodes in the economic growth and industrial revolution [1]. Subsequently, a sufficient and continuously available electrical energy supply is the main block of a long-term civilization and its financial matters [2].

Due to a growth in the number of users and the emergence of high-power sectors, electrical energy demands have increased drastically over the past few decades. Subsequently, this traditional energy generation has resulted in a considerable increase in environmental pollution [3], [4]. As a result, there has been a tremendous rise in deploying small-scale and

The associate editor coordinating the review of this manuscript and approving it for publication was N. Prabaharan.

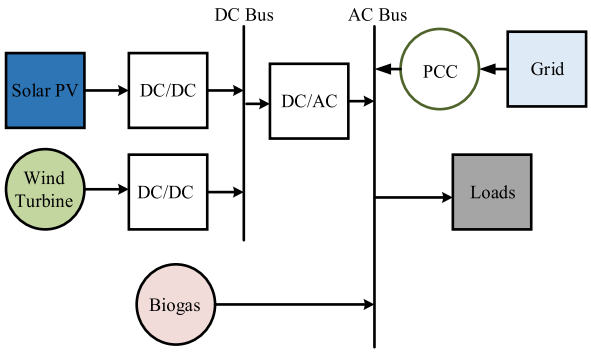

FIGURE 1. A generic RES-based microgrid system.

large-scale green energy resources into the electricity system. Resultantly, the world witnessed the transition of the Powers system from conventional energy resources (furnace oil, coal, etc.) to renewable energy resources (RES), which are also called non-conventional energy resources, in the last couple of decades [5]. A generic RES-based microgrid system is shown in Fig. 1.

Due to the sudden increment of RES and shift of the industrial sector toward non-conventional resources like solar, wind, micro-hydro biogas, and other renewable resources [6], [7], subsequently, the research deviates toward improving power electronic converters. Through this, the network operators should maintain the reliability and stability of the power system under predefined constraints [8], [9], [10].

Multi-level inverters (MLIs) have been around for over three decades and continue to get the most interest from researchers in business and academia since they are proven to be more favorable than their two-level inverter predecessors [11]. Minimum switching losses, reduced harmonic content, little electromagnetic interference, lower-rated switches, reduced voltage stress on switches, high-quality output waveform, and improved efficiency are some of their advantages [12]. Renewable energy systems, electric drives, hybrid electric cars, flexible alternating current transmission systems (FACTS), reactive power compensation, and high voltage direct current (HVDC) all are applications getting benefits from multi-level inverters [13], [14].

A vast research effort has been made over the last couple of decades to produce multi-level inverters with a lesser number of switches and a minimal number of dc sources [15], [16]. For example, the authors of [17] presented the three-phase three-level neutral point clamped inverter along with the MPPT algorithm to extract maximum power from the photovoltaic system. The system relates to a common DC-link so that there is no need for a DC-DC converter, while a synchronous reference frame (d-q) control strategy was applied to control current and dc-link voltage. However, this research could not explain the efficiency of THD in output voltage and current.

The authors in [18] presented the comprehensive analysis of 3 types of multi-level inverters named 5, 7, and 9 levels using phase disposition pulse width modulation technique and compared with simple pulse width modulation technique. These researchers concluded that with the SDPWM technique, the THD content in output voltage and the current reduced considerably. However, this technique required more switches, which may increase both conduction and switching losses and affect the THD content in both voltage and current profiles.

Another research effort [19] was carried out in the context of the analysis and design of 13 level hybrid cascaded multi-level inverter utilizing the combined sinusoidal pulse width modulation (SPWM) and selective harmonic elimination (SHE) technique to minimize the percentage of total harmonic distortion and improve the voltage and current profile. The ratio of 1:2:4 of dc voltage sources was utilized, and the THD of 9.29% without the SHE technique while 6.19% with SHE was recorded. However, this research was unable to address the loading effect on the inverter's output voltage profile and did not include the inductive loading effect. The suggested work in [20], [21], and [22] design an inverter topology using five, seven, and eleven levels respectively. Due to a smaller number of levels, the maximum THDs reduction achieved in these research works is up to 7 percent on resistive loads, on inductive loads the THDs and losses are increased further. In [20], the 5-level inverter is designed by using 8 switches and due to large number of switches, the inverter efficiency may reduce. No comments were made about the inverter efficiency and ANN architecture and its complexity. In [21], the algebraic method was utilized along with ANN to reduce the THDs. The main drawback of this approach is to large number of neurons (280) in the hidden layer and more than one outputs were also reported on the same modulation index values. In [22] the main focus was on the accuracy improvement of the ANN which was achieved by using quasi-newton method along with ANN. But the space complexity of quasi-newton methods is $O(n^2)$ and they involve dense matrices hence their time complexity is also $O(n^2)$ [23] for each iteration. Moreover, the proposed MLI topology, number of switches, losses, and efficiency is not discussed in the paper.

The authors in [24] presented the comparative analysis of different control techniques for a three-phase 17-level inverter with two cascaded square bridges. This research work proposed a square bridge topology to produce said levels utilizing various techniques like phase disposition (PD), phase opposition disposition (POD), and alternative phase opposition disposition (APOD) with different modulation indexes (Ma) under different loading conditions (Resistive only, resistive-inductive only, RLC, etc.) to see the effect on the harmonic content of output voltage and current profile. However, the switching losses and conduction losses should be appropriately analyzed in efficiency at high switching frequencies. In [25], the authors have proposed an eleven-level CHB-MLI which is also using PD and APOD techniques along with a PI controller. The proposed MLI was compared with conventional MLIs and found to be better in terms of

THD levels, however, efficiency is not calculated at different types of loads. The authors in [26] presented the 23-level multi-level inverter with a new control technique named the sinusoidal tracking technique. Analysis was done only for resistive load with different switching angles to produce optimum angles with minimized THD content.

The [27] presented the fuzzy logic-based PWM control technique for 27 levels asymmetric multi-level inverter for lower power applications. The proposed model utilized different dc voltage sources, and at the same time, both positive and negative voltage sources accommodate to produce desired levels. This technique may work well for resistive loads. However, for inductive loads, it may not be able to deliver desired output as inductive load generates a back-EMF voltage now when the switches are turned on or off. Due to this, the peak voltage is much greater than the voltage that the load AC power supply can withstand, which can easily cause the inverter in overload condition to shorten inverter life. Another fuzzy logic-based MLI is proposed in [28]. The proposed topology is designed to produce 11 levels and with a low number of levels, this study has reported relatively higher THDs. Moreover, the fuzzy logic approach may also accept the wrong/less accurate input, which is why the output waveform is sometimes less accurate/unreliable.

The topology and algorithm proposed in [29] is the reference for this research work. In [29], the authors have presented the novel 27-level multi-level inverter with the Phase Shifted-Modified Synchronous Optimal Pulse Width Modulation technique. The proposed topology incorporated the built-in induction motor model in their simulation. However, the H-bridges were included in both positive and negative cycles at a similar time which may not work correctly in high inductive loading. The reason for this is well explained in the above paragraph. Also, the THD percentage seems to be high compared to the proposed levels. Another switched capacitor-based topology for CHB MLI is presented in [30] which uses only one DC source, but the main drawback of this technique is the capacitor inrush current. A Genetic Algorithm (GA) based MLI is presented in [31] which can be used in two modes. The first mode is battery charging and the second is the inverter. In the proposed topology, the GA is used to find the optimum switching angles to reduce the switching losses. However, the inverter is having only 7 levels.

It is evident from the literature that most of the CHB MLIs either have a smaller number of levels or use a greater number of switches to achieve a higher number of levels. In order to reduce the THD levels the switching angles are adjusted. Most common switching angle calculation methods are equal phase (EP), half equal phase (EHP), half height (HH), and feed forward (FF) [32]. None of these methods guarantees the lowest THD levels hence we need the optimization techniques. Some AI-based approaches are using fuzzy logic or GA to calculate the switching angles. The fuzzy-based systems may accept inaccurate data at the input, hence may result in a wrong output for GA the time complexity of the algorithm depends on the fitness function [33] and for a nonlinear equation of order 5, the complexity becomes $O(n^5)$ which makes the response time very high. Hence a more efficient approach is necessary to design the CHB-MLI with a greater number of levels and a smaller number of switches.

The current research effort has some unique points, which are as follows:

- Utilization of an improved ANN architecture for THD reduction.
- The proposed ANN has better performance in overfitting and underfitting situations.
- Obtaining 15 levels without incorporating opposite polarities of DC voltage sources.
- Getting better THD performance as compared to [29] by using less number of switches.
- The proposed model comprises PV integration with the proposed MLI inverter.

Our contribution to this paper is the utilization of the ANN technique to find the optimum switching angles for the proposed MLI that ensures the minimum possible THD levels. The use of ANN will result in the reduced response time of the MLI as the model will be trained only once, and then the optimum switching angles can be calculated in every case. We are using only hidden layers and the output layer in our ANN, hence the complexity of the proposed technique will be $O(n^2)$ [34] which is better than the existing approaches. Furthermore, the THD levels at current are reduced to 2.9% as compared to 10.94% in the [29]. Similarly, the THD levels in voltage are also reduced to 5.94% as compared to 6.9% previously reported in [29]. These improvements are made by using the same number of switches and more feasible ratios of DC sources. The efficiency of the proposed model is also computed to be 89.6% and the simulation results are verified.

In this research work, our proposed methodology can be applied to multiple renewable energy resources, as this research work is based on designing an optimal multi-level inverter using an ANN network architecture, which can be integrated with multiple renewable energy resources, as depicted in Fig. 1. Any scientific researcher in the future can easily extend this model in case of utilizing any renewable energy resource that can be easily integrated with the multi-level inverter designed in this research work [35].

The structure of this document is as follows. The research methodology for the proposed fifteen-level MLI is presented in Section II. Switching and power losses are computed in section III. Meanwhile, all the results are presented in section IV, where the suggested MLI model is also compared to the classical model and the reference paper. Followed by a conclusion in section V.

II. METHODOLOGY

An asymmetric CHB configuration of a 15-level cascaded H-bridge multi-level inverter is developed in MATLAB/Simulink, where it is powered by three isolated solar PV arrays. Furthermore, three different cascaded H-bridges are also developed in this proposed model. Moreover, ANN

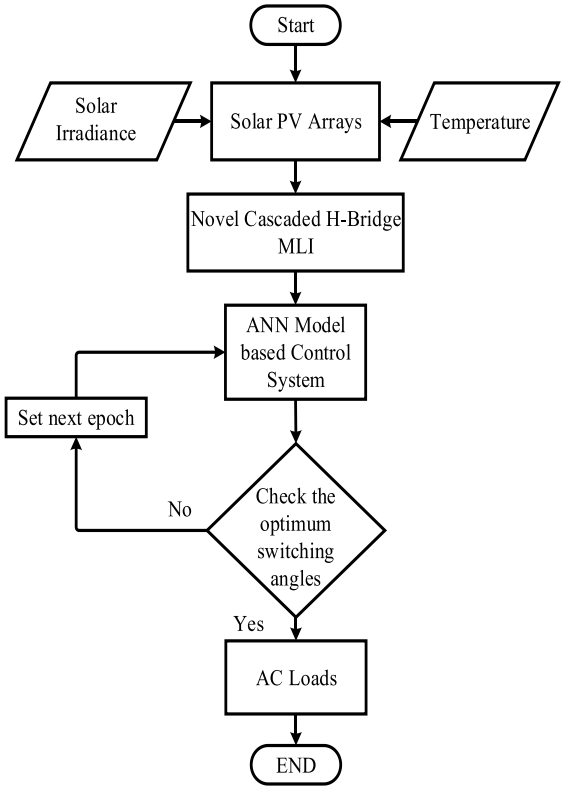

FIGURE 2. Flow diagram of the proposed MLI system.

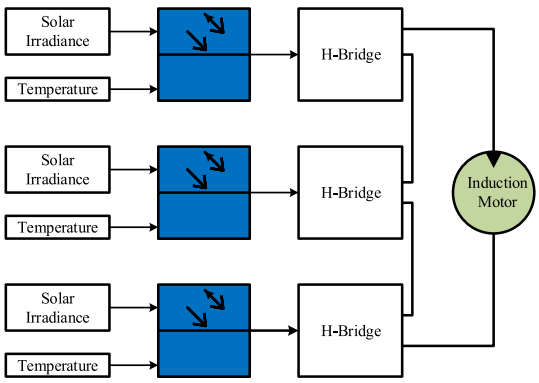

FIGURE 3. Block diagram of the proposed MLI system.

is used as a control algorithm to find the optimum switching angles of the proposed MLI. A flow diagram is shown below in Fig. 2 to explain the working of the suggested system, which is divided into three major groups, i.e., solar PV arrays, proposed fifteen-level cascaded H-bridge MLI, and three-phase AC loads.

The block diagram of the proposed system is shown below in Fig. 3, consisting of the temperature and irradiance blocks, and inverter blocks connected in cascaded connections. We have tested our proposed topology on an inductive load; hence an induction motor is used as a load in fig. 3.

A. PROPOSED 15-LEVEL CASCADED H-BRIDGE MLI

The proposed model is designed to produce fifteen-level output, i.e., seven positive, seven negative, and one zero level, using only three H-bridges, which means only twelve IGBT modules are used. Therefore, it is considered the primary motivation of this proposed model. Trina solar TSM-250PA05.08 panel is used to develop the three isolated PV arrays of peak ratings of 250W, 500W, and 1000W, which have been integrated with the proposed MLI system to power all the H-bridges with a specific output voltage ratio of 1:2:4. Meanwhile, all these PV panels are operated at standard irradiance and temperature conditions, i.e., 1000w/m2 and 25°C, respectively. The technical specifications of the panel used in this modeling are given below in Table 1.

TABLE 1. Technical specifications of "trine solar TSM-250PA05.08".

Quantity	Value
Model Name	"Trina solar TSM-250PA05.08 panel"
Type of cell	Polycrystalline cell, six-inch
Maximum nominal power rating	250 Watt
Maximum operating voltage rating (V_{mp})	31 Volt
Maximum operating current rating (I_{mp})	8.06 Ampere
Open circuit voltages rating (V_{OC})	37.5 Volt
Short circuit current rating (I_{SC})	8.55 Ampere
standard Irradiance	1000 watts/m^2

Moreover, the reference model in [29] has also used three H-bridges that are operated in both positive and negative cycles simultaneously to produce maximum output levels (i.e., 27 levels). For example, to produce the 2nd output level, the 1st H-bridge is operated in a positive and the 3rd H-bridge in a negative (i.e. $(1) + (-3) = 2$), which doesn't work well at inductive loads. However, the proposed model is designed in such a streamlined way that there is no need to operate H-bridges in negative to produce positive output levels, which is equally efficient to be used with both resistive and inductive loads. Overall, the ratio of the isolated solar PV arrays is shown below:

$$Vpv1 : Vpv2 : Vpv3 = 1 : 2 : 4 \tag{1}$$

Subsequently, the first H-bridge can produce three output levels: $+1{*}\mathrm{V}pv$, $0{*}\mathrm{V}pv$, and $-1{*}\mathrm{V}pv$. While a second bridge can produce $+2{*}\mathrm{V}pv$, $0{*}\mathrm{V}pv$, and $-2{*}\mathrm{V}pv$ and the third bridge can produce $+4{*}\mathrm{V}pv$, $0{*}\mathrm{V}pv$, and $-4{*}\mathrm{V}pv$. The mathematical representation is given below:

$$V_{pv1} = \begin{cases} +1 * Vpv \\ 0 * Vpv \\ -1 * Vpv \end{cases} \tag{2}$$

$$V_{pv2} = \begin{cases} +2 * Vpv \\ 0 * Vpv \\ -2 * Vpv \end{cases} \tag{3}$$

$$V_{pv3} = \begin{cases} +4 * Vpv \\ 0 * Vpv \\ -4 * Vpv \end{cases} \tag{4}$$

TABLE 2. Switching control of the proposed fifteen-level cascaded H-bridge MLI.

Positive half cycle		Negative half cycle	
V_{out}	Vpv_1+Vpv_2+Vpv_3	-V_{out}	-Vpv_1-Vpv_2-Vpv_3
1	1+0+0	-1	-1+0+0
2	0+2+0	-2	0-2+0
3	1+2+0	-3	-1-2+0
4	0+0+4	-4	0+0-4
5	1+0+4	-5	-1+0-4
6	0+2+4	-6	0-2-4
7	1+2+4	-7	-1-2-4

The switching control of the proposed fifteen-level cascaded h-bridge is shown in Table 2.

B. ARTIFICIAL NEURAL NETWORKS (ANN) BASED INVERTER CONTROL

Artificial neural networks (ANN) is an artificial intelligence-based technique used as an intelligent controller [36] to find the ON/OFF control value for the optimal switching of the IGBT switches used to develop the proposed MLI in Simulink. The leading cause behind using ANNs is their nature, like a biologically-inspired computer program [37]. This model is designed to simulate a manner similar to what the human brain does to process information. By detecting the patterns and relationships in data, ANNs collect their knowledge and then learn (or are trained) through detected patterns, not programming [38]. Subsequently, this intelligent model is developed using a single time series input, ten hidden layers (i.e. each hidden layer consists of ten neurons), and one output layer (i.e., twelve output control signals to switch the IGBT modules). Connecting neurons in a network gives power to neural computations. Each neuron carries weighted inputs, one output, and a transfer function. The behavior of a neural network is decided through the transfer functions of its neurons, by the learning rule, and by the architecture itself [39]. A parameterized system is one whose weights can be adjusted [40]. Since we can adjust the weights of ANN, it is considered a parameterized system. The weighted sum of the inputs causes the activation of the neurons. The activation signal is later gone through the transfer function [41], resulting in a single output of the neuron. These transfer functions usually introduce non-linearity to the network. The method of describing input-output relation in a non-linear method is a task of activation function [42]. This gives the model ability to describe an association between its inputs and outputs. The purpose of the activation function is to map the output of every weight input multiplication in a range that helps in firing or not firing a particular neuron. If the value given by the activation function is below some threshold value, the neuron will not fire, and a zero is passed to the next layer. In the other case, the neuron fires, and the output of this layer is multiplied by the weight of the next layer and the process continues in the forward loop until we reached the output layer and calculated some error. Commonly reported activation functions are Sigmoid [43], ReLU [44]., Tanh, and Softmax [45]. We used ReLU as an activation function in our system. The reason for using ReLU is its ability to activate neurons without being computationally expensive to the system.

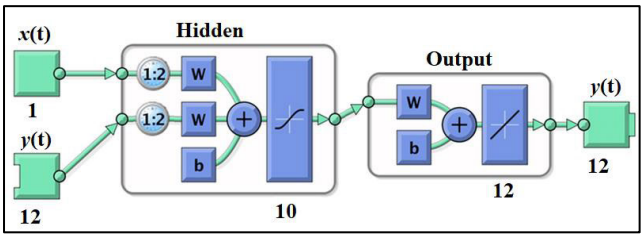

FIGURE 4. A detailed structure of the Proposed ANN model.

Moreover, in our design, we used seventy percent data for training. During training, the inter-unit connections are optimized until our network reaches the required accuracy level and the prediction error is minimized. In case of an error, weights get updated. Error in the sense of wrong classification or misclassified things. The weight updating equation used in the model is:

$$weight = weight + learning_{rate} * (expected - predicted) * input$$

A score or prediction for each input provided to the system is the network's output. The loss function is there to measure the performance of the predictor. A loss will be high if the predicted class does not match the actual result. It will be low the other way around. Overfitting and underfitting problems might occur at the time of training. In the case of overfitting or underfitting, our model performs relatively better on training data but gives a poor performance on testing data. During network training, we need a loss function or optimizer or some dropout layers. This will find a value of the weight that minimizes the loss.

Of the rest of the thirty percent of data, fifteen percent of data is used for validation and fifteen percent for testing. The overall structure of the proposed ANN model, which is developed in MATLAB/Simulink, is given below in Fig. 4. Pseudocode of how the learning weight value is updated in the implantation is explained below:

C. CALCULATION OF SWITCHING ANGLES

Various switching angle modulation techniques are used to control the voltage waveform output of the multilevel inverter. These modulation techniques can be divided into two groups based on the switching frequency of power semiconductor devices: a) low switching (fundamental) frequency and b) high switching frequency. Space Vector Control (SVC) and Selective Harmonic Elimination (SHE) are low-frequency techniques [46]. In the CHB-MLI, the output voltage waveform is given by the sum of the output voltages generated by each H-Bridge module connected in series [47]. The

Initialization of w: w ← 0.27; // variable w for weight value. Its initialization is random to start the learning.
for i ← 1 to predefined iteration number
$\Delta w_i \leftarrow 0$; // change of weight initialize to zero before the start of every loop iteration
while (there is training data available) **do:**
te ← to find and store the current training example;
row ← to find and store the row number from the matrix (te);
col ← to find and store the column number from the matrix (te);
out ← to find and store the network output (te);
maxSimRow ← to find and store the maximum similarity in a row (row);
maxSimCol ← to find and store the maximum similarity in column (col);
Δw_i will be updated using the below equation:

$$\Delta w_i = \Delta w_i + \eta\left[(\text{maxSimRow} - \text{out}) + (maxSimCol - out)\right];$$

remove current training data();
end
$\Delta w_i \leftarrow w_i + \Delta w_i$;
restore training example from the temporary variable te();
end;

Fourier series expansion technique is used to analyze the inverter's output voltage waveform. In general, the Fourier series expansion can be expressed as [48]:

$$v_{out} = \sum_{n=1}^{\infty} \frac{4V_{dc}}{n\pi}\left[\sum_{k=1}^{s}\cos\left(n\alpha_k\right)\right]\sin\left(n\omega t\right) \tag{5}$$

In the above equation:
n = odd harmonic order (1, 3, 5, 7, …)
s = number of stages in the MLI
k = a positive integer
α_k = switching angle for kth switch
Here the switching angles must satisfy the following relation:

$$\alpha_1 < \alpha_2 < \alpha_3 \ldots < \alpha_s < \pi/2 \tag{6}$$

From equation (5) The amplitude of the odd harmonics, including the fundamental component, can be expressed as follows:

$$a_n = \frac{4V_{dc}}{n\pi}\sum_{k=1}^{s}\cos\left(n\alpha_k\right) \tag{7}$$

By expanding the above equation, we get:

$$a_n = \frac{4V_{dc}}{n\pi}\left[\cos\left(n\alpha_1\right) + \cos\left(n\alpha_2\right) + \ldots + \cos\left(n\alpha_s\right)\right] \tag{8}$$

The goal of calculating the optimal switching angles is to minimize the output voltage's total harmonic distortion. The neural network problem can be expressed as:
Decision variables are: $\alpha_1, \alpha_2, \ldots, \alpha_n$ with the restrictions given in (6).
The objective function can be expressed as:

$$THD\,(\%) = \left[\left(\frac{1}{a_1^2}\right)\sum_{n=3}^{\infty} a_n^2\right]^{1/2} \times 100 \tag{9}$$

where:
a_1 is the fundamental amplitude
a_n is the amplitude of the nth harmonic
Our goal is to minimize the objective function given in (9).
The flowchart of the proposed algorithm is shown in fig. 6 below.

III. ESTIMATION OF POWER LOSSES

In a Multilevel Inverter, calculating power losses is critical for cost assessment and construction cooling systems. Conduction losses and switching losses are two different forms of power losses. Conduction losses are prominent at low switching frequencies, but switching losses are significant at high switching frequencies. Any number of levels can be added to the MLI idea. Because the number of switches is proportional to the number of levels.

The power loss will rise as the number of switches increases. In this study, we have produced more levels by using a smaller number of switches which proves that the proposed design will be having fewer power losses as compared to traditional MLI configuration. Loss calculations are also required to demonstrate the efficacy of the proposed design. The two basic forms of losses associated with power electronic switches are conduction loss (P_{cl}) and switching loss (P_{sl}). The total switching losses (P_l) may be determined by summing the conduction and switching losses of each switch, as shown in equation (10) below:

$$P_l = P_{cl} + P_{sl} \tag{10}$$

A. SWITCHING LOSSES

The switching losses are calculated for a single switch and then extended to other switches as shown in [49] and by using the linear approximation given in [50] and [51] the energy loss during the turn-off and turn-on period can be calculated. Switching losses may be computed by multiplying the frequency by the sum of energy losses in each switch, as shown in the equation below:

$$P_{sl,k} = f\sum_{k=1}^{N}\left[\left(E_{off,k} + E_{on,k}\right)\right] \tag{11}$$

Here $P_{sl,k}$ is the switching loss in the kth switch, f is the frequency, $E_{off,k}$ is the energy during the turn-on period and $E_{on,k}$ is the energy during the turn-off period for the kth switch. The expressions of energies during the turn-off and turn-on period can be given as:

$$E_{off,k} = \int_0^{t_{off}} v\left(t\right) i\left(t\right) dt = \frac{1}{6}\left(v_{SW,k} \times I \times t_{off}\right) \tag{12}$$

$$E_{on,k} = \int_0^{t_{on}} v\left(t\right) i\left(t\right) dt = \frac{1}{6}\left(v_{SW,k} \times I' \times t_{on}\right) \tag{13}$$

In the above equations, t_{off} and t_{on} are the turn-off and turn-on times for the switch k respectively. Off-state voltage is

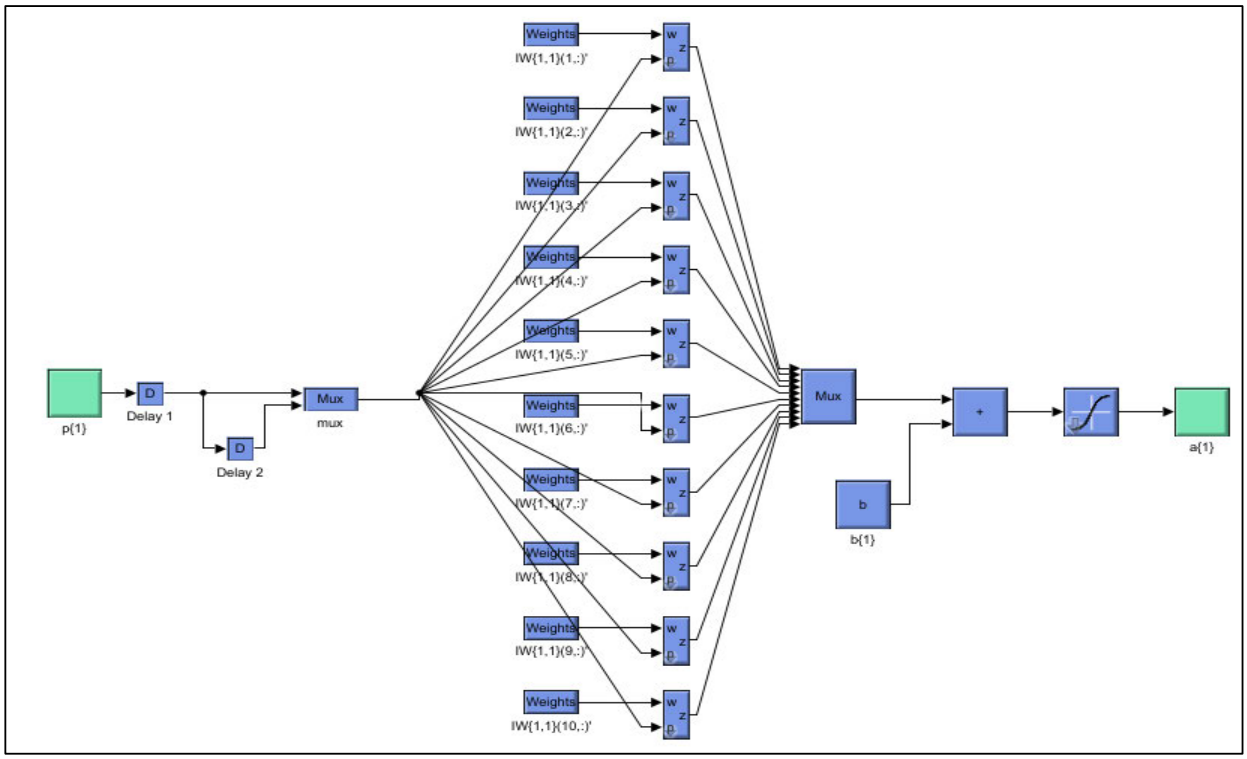

FIGURE 5. Structure of the one hidden layer of the proposed ANN model.

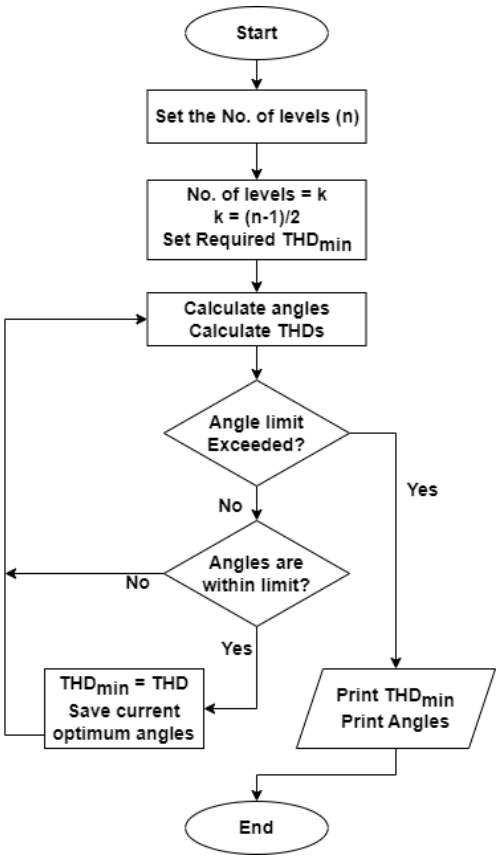

FIGURE 6. Flowchart of algorithm for calculating switching angles.

shown by $v_{SW,k}$, I′ is the current in the switch after turning on and I is the current through the switch before turning off.

B. CONDUCTION LOSSES

As stated in [50], the conduction losses are caused by the on-state voltage drop of the switch and equivalent resistance. An example switch is used to evaluate conduction losses, which is then applied to other switches in the proposed MLI. As there is an anti-parallel diode, so the conduction losses will exist in both switch and the anti-parallel diode. And the total conduction loss is the sum of both these losses for a given switch k. The expression of conduction loss can be given as:

$$P_{cl,k} = \sum_{k=1}^{N} \left(P_{cl,t,k} + P_{cl,d,k}\right) \tag{14}$$

Here $P_{cl,t,k}$ is the conduction loss at switch k, and $P_{cl,d,k}$ is the conduction loss at the anti-parallel diode k and these losses can be computed by using the equations (15) and (16) respectively.

$$P_{cl,t,k} = \left[\left(V_t \times I_{t,avg}\right) + \left(r_t \times I_{t,rms}^2\right)\right] \tag{15}$$

And the anti-parallel diode losses can be computed as:

$$P_{cl,d,k} = \left[\left(V_d \times I_{d,avg}\right) + \left(r_d \times I_{d,rms}^2\right)\right] \tag{16}$$

In the above equations, V_t is the on-state voltage drop across the switch, and V_d is the on-state voltage drop across the anti-parallel diode. r_t is the collector-emitter on-state resistance of the switch and r_d is the on-state resistance of the diode. I is indicating the current in the diode and switch during the on-state. Here we are considering both the average current and the RMS current as indicated by the subscripts. And finally,

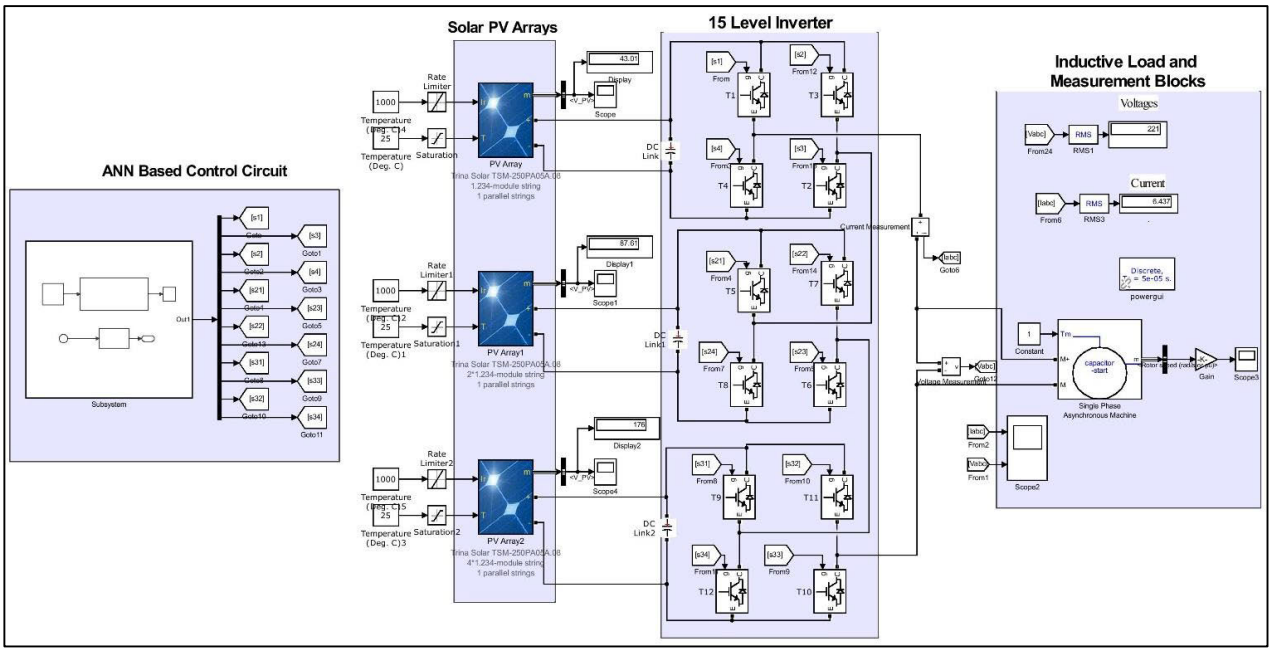

FIGURE 7. Complete simulink model of the proposed fifteen-level cascaded H-bridge MLI.

TABLE 3. Losses and efficiency at inductive load.

Parameters	Value
V_{rms}	221 Volts
I_{rms}	6.437 Amp
P_{out}	1422.58 Watt
$P_{cl,t}$	101.71 Watt
$P_{cl,d}$	62.76 Watt
P_{cl}	164.47 Watt
E_{on}	0.27 Watt
E_{off}	0.405 Watt
P_{sl}	0.675 Watt
P_l	165.145 Watt
P_{in}	1587.73 Watt
Efficiency	89.6%

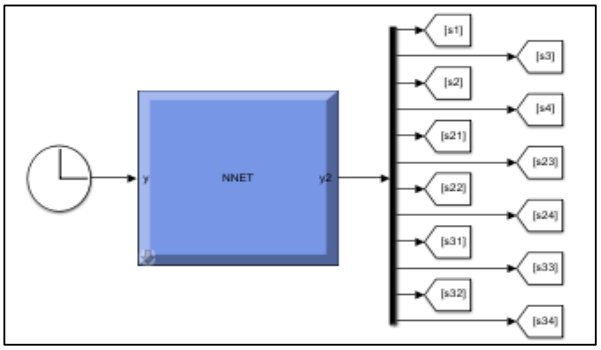

FIGURE 8. Overall ANN subsystem block in simulink model.

the efficiency can be calculated as:

$$\eta = \frac{P_{out}}{P_{out} + P_l} \times 100 \tag{17}$$

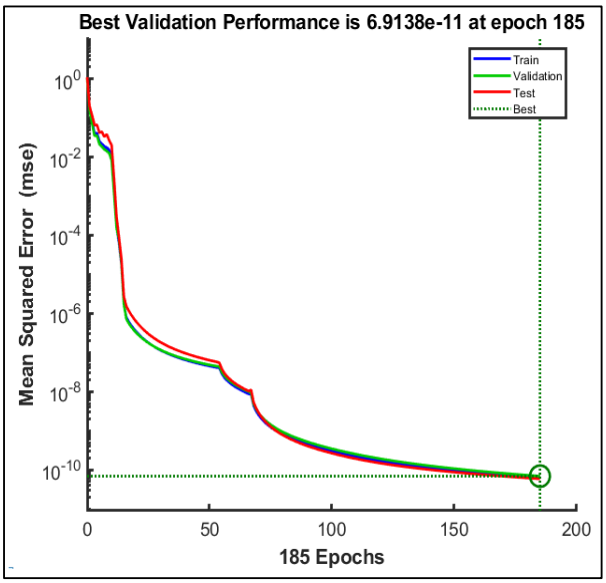

FIGURE 9. Error plot of the proposed ANN model.

All these losses were calculated by using equations (10) through (16). The following values were estimated for the calculations.

$$V_t = 2.5V, V_d = 1.5V, r_t = 0.15\Omega,$$
$$r_d = 0.12\Omega, t_{on} = t_{off} = 80\mu s$$

The simulation was carried out by using an inductive load and all the calculated losses and the efficiency is given in Table 3 below.

IV. RESULTS AND DISCUSSIONS

To obtain the desired configuration of a fifteen-level cascaded H-bridge multi-level inverter, the proposed model is

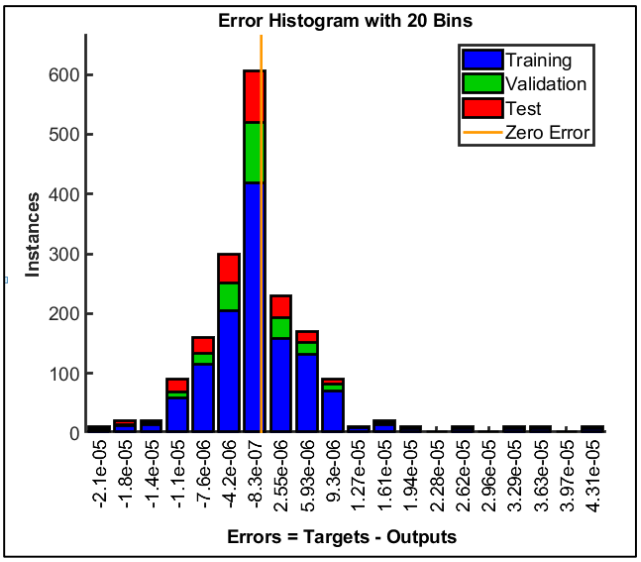

FIGURE 10. Error histogram of the proposed ANN model.

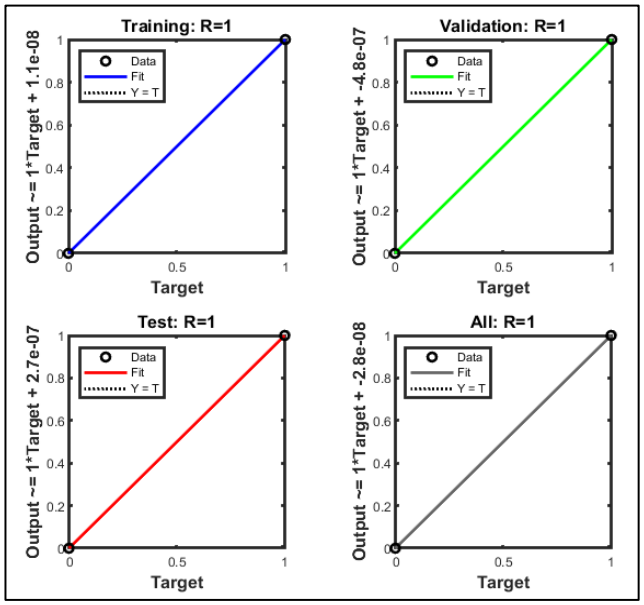

FIGURE 11. Regression curves of the proposed ANN model.

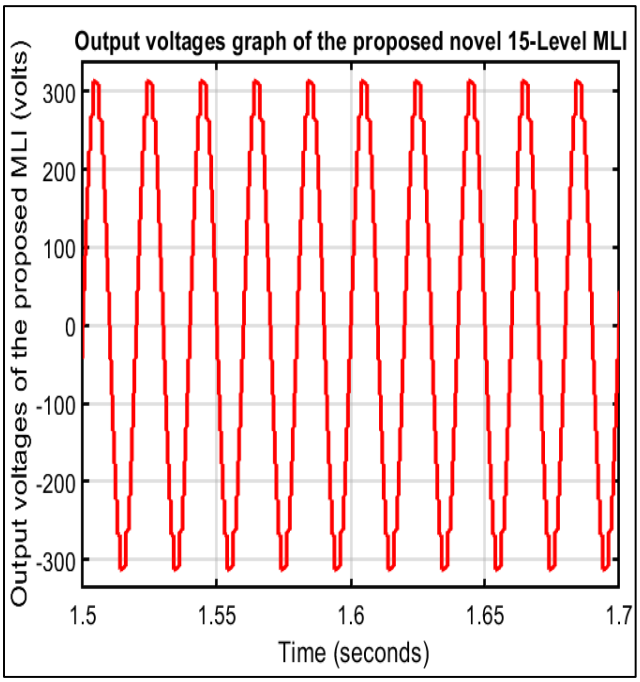

FIGURE 12. Output voltages of the fifteen-level cascaded H-bridge MLI.

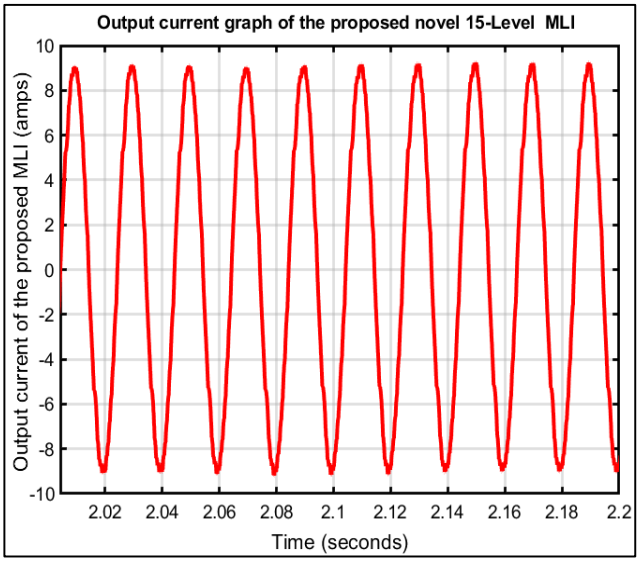

FIGURE 13. An output current of the fifteen-level cascaded H-bridge ML.

employed in Simulink in four different parts (i.e., Solar PV arrays, cascaded H-bridges, ANN-based control unit, Induction motor as a load). Meanwhile, three cascaded H-bridges are used to complete the design model, with each bridge including four distinct IGBT switches. These H-bridges are powered by the three isolated solar PV arrays in a specific voltage ratio of 1:2:4 to achieve the required fifteen-level output. This model presently employs eight independent PV arrays, although any of these arrays can be replaced. As specified in the design, continuous DC voltage sources should be used instead. Moreover, artificial neural networks are used to predict the optimal switching of the angles of the IGBT switches used in the configuration of this MLI. The structure of the one hidden layer of the proposed ANN model is shown in Fig. 5 above, whereas the overall Simulink model is shown in Fig. 7 below.

The first part of the Simulink model shown above is the ANN-based control unit. Meanwhile, this control unit is developed using the MATLAB app of a series neural network. Moreover, this model is trained using the one hundred and fifty-six different switching states at different time steps. The complete structure of this model is shown above in the methodology section. However, the overall subsystem block

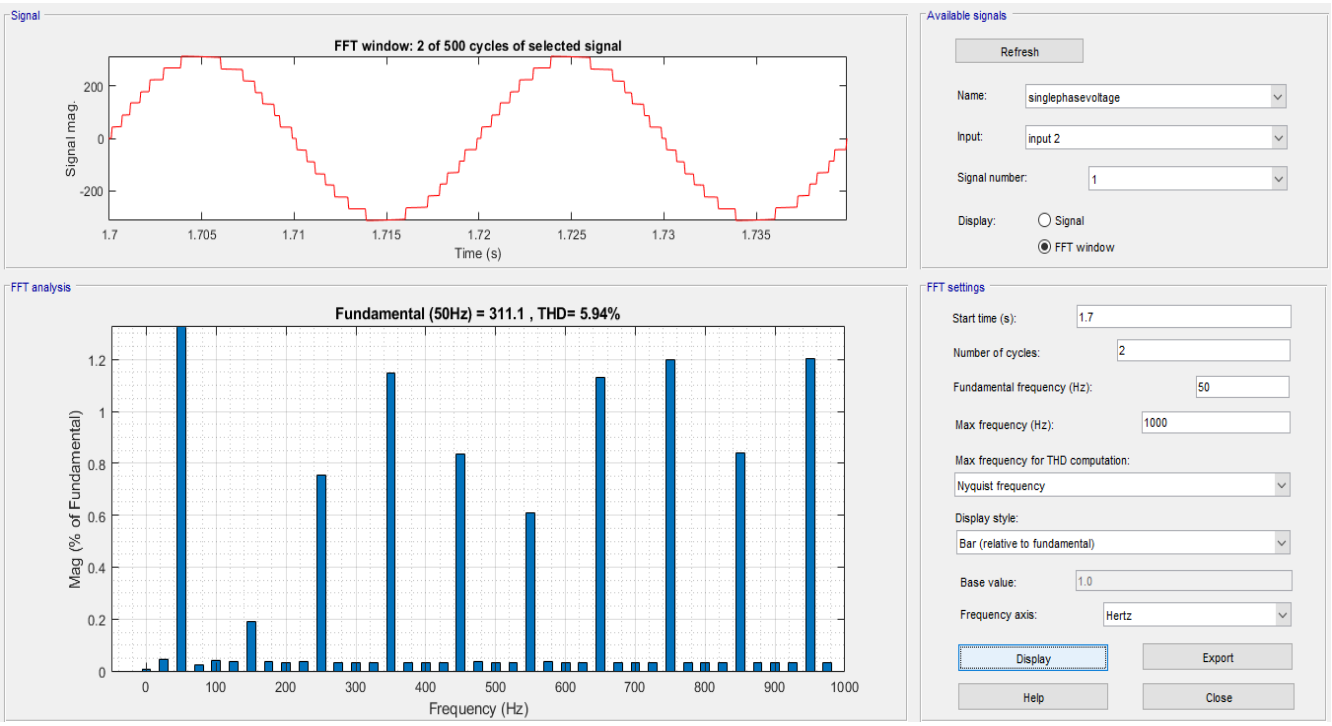

FIGURE 14. THD analysis of the output voltages of the fifteen-level cascaded H-bridge MLI.

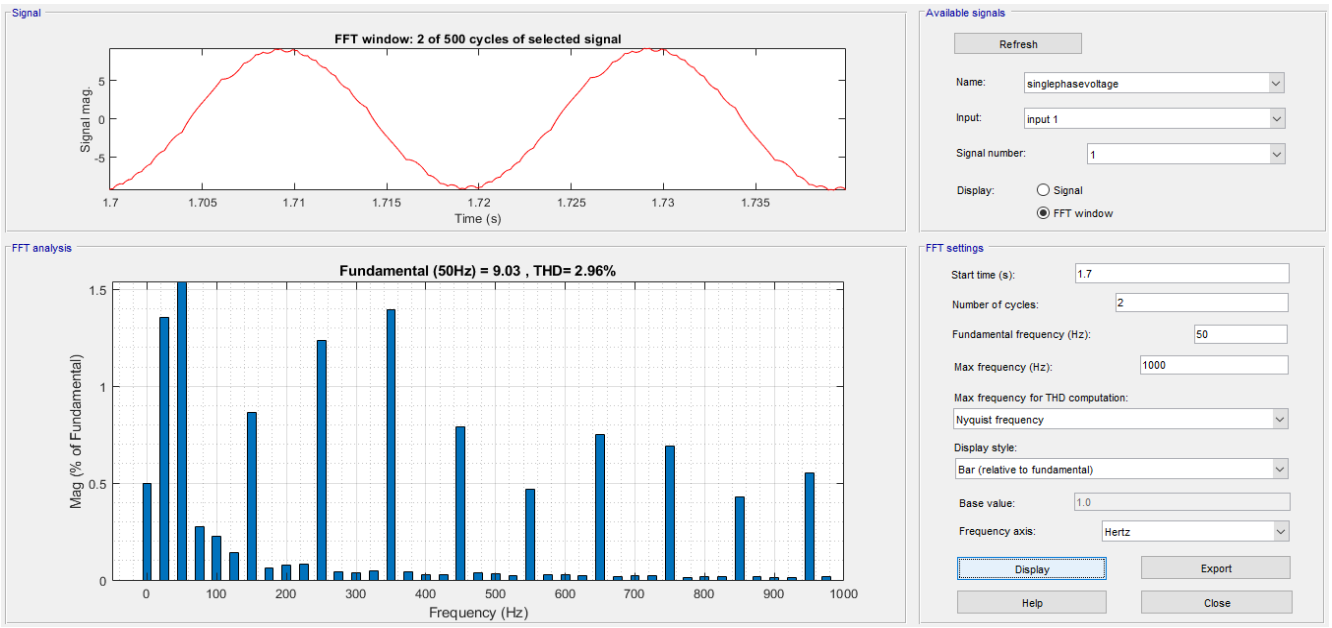

FIGURE 15. THD analysis of the output current of the fifteen-level cascaded H-bridge MLI.

is shown below in Fig. 8. Its input is the time clock, and the output is separated into twelve using the demux block.

A. PERFORMANCE OF THE ANN MODEL

The ANN model's performance assessment is evaluated by plotting the error graph. This model is set to run through a momentum algorithm, in which it doesn't stop passing through the next epoch until the best error values are achieved. Subsequently, this proposed model achieved its best performance with the slightest error after passing through one hundred and eighty-five epochs. The error plot is shown below in Fig. 9. The blue line represents the training data error, the green line represents the validation data error, and the red line represents the testing data error. Moreover, it can

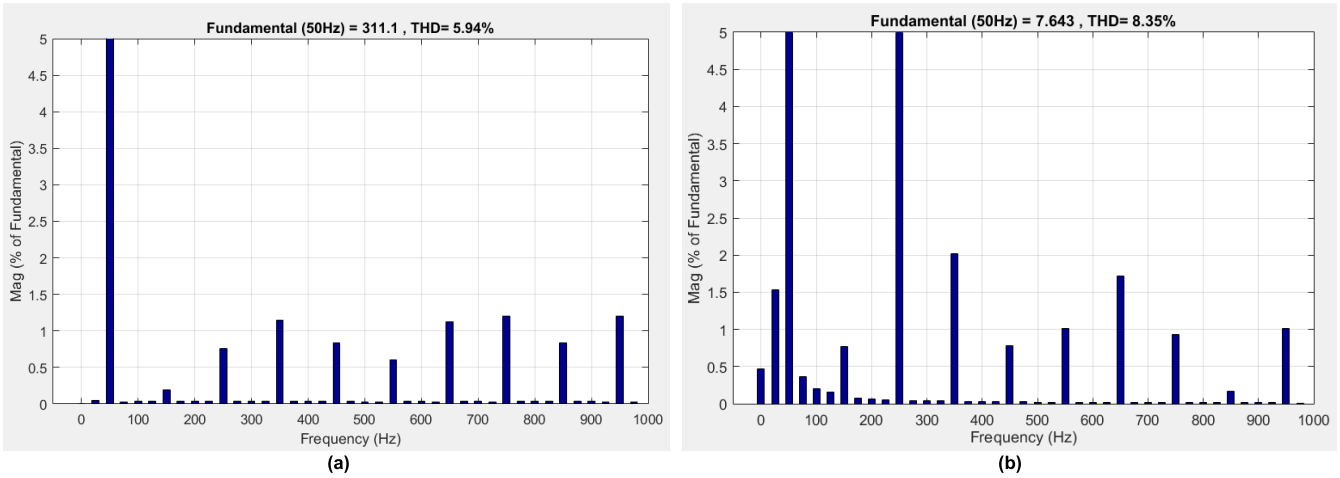

FIGURE 16. Comparison of voltage signal THD levels (a) with ANN (b) without ANN.

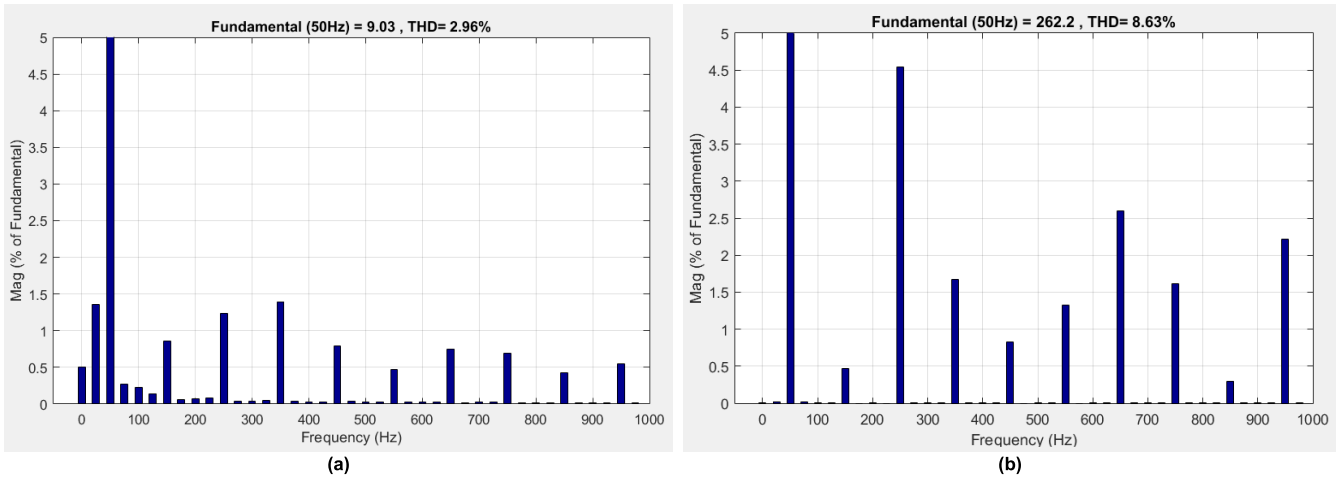

FIGURE 17. Comparison of current signal THD levels (a) with ANN (b) without ANN.

also be seen that all three types of error overlap at the best values shown in Fig. 9, representing the best fitting of the proposed model.

The system's error histogram is also shown below in Fig. 10. The training, validation, and testing errors are represented in blue, green, and red, respectively. As the number of cases arises, the error for the testing set became higher.

The used ANN model's regression curves are shown in Fig. 11, which shows the training, validation, and target data regression curves in one figure. Meanwhile, the circles show the data values, and the solid line shows the fit line. If the data values lie on the fit line, then the data is trained precisely; if they are below or below the fit line, the data has some error. Conclusively, Fig. 11 represents that all the data values are on the fit line, resulting in the best model performance.

B. PERFORMANCE OF THE PROPOSED FIFTEEN-LEVEL CASCADED H-BRIDGE MULTILEVEL INVERTER

The proposed configuration of a fifteen-level cascaded H-bridge multi-level inverter converts the DC output of the solar PV arrays into AC output at fifteen levels by using the ANN-based ON/OFF control of the IGBT switches. Moreover, this proposed system has achieved the fifteen-level voltage output by using only twelve switches, which helped it reduce the cost and switching losses. As a result, the system has reached a lesser THD value equal to 5.95 percent, as suggested in the above sections. The output voltages and current of the fifteen-level cascaded H-bridge MLI are shown below in Figs. 12 and 13, respectively.

The THD curves of the proposed system's voltage and current are shown below in Figs. 14 and 15, respectively. A comparison of THDs with and without using the ANN is also given in Figures 16 and 17 respectively. Figure 16 represents the THD levels in the voltage signal, and figure 17 represents the THD levels in the current signal with and without ANN.

It can be noticed from figure 16 (b) that, the voltage signal THDs are at 8.35% by using the HEP method. But after optimizing the switching angles with the help of ANN, the THDs reduced to 5.94% as shown in figure 16 (a) indicating a 28.86% improvement in the voltage THDs. Similarly,

TABLE 4. Comparison with the previous proposed work.

	Conventional multi-level inverter	Recent Model [28]	Reference model [29]	Proposed model
Output levels	15	15	27	15
Number of switches	28	14	12	12
Number of solar arrays	7	7	3	3
The ratio of DC sources	1	1	1:3:9	1:2:4
THD in voltages	Higher	7.97%	6.9%	5.94%
THD in current	Higher	5.49%	10.34%	2.9%

figure 17(b) is showing 8.63% THDs in the current signal when ANN was not used, but with the use of the ANN technique, the THDs in the current signal is reduced to 2.96% as depicted in figure 17(a). Hence ANN caused a 65.70% improvement in the THDs of the current signal for the proposed MLI.

C. COMPARISON WITH THE REFERENCE MODEL [29]

The reference model in [29] is also a similar configuration of the cascaded H-bridge multi-level inverter powered by the solar array with a specific ratio of 1:3:9. Moreover, this reference model also contains a PWM technique to optimize the switching control resulting in the THD level of voltage and current signal up to 6.9 percent and 10.34 percent respectively at inductive loads. Meanwhile, the proposed ANN-based MLI configuration proposed in this paper is designed with a specific input DC voltage ratio of 1:2:4 and it achieved the THD values of 5.94 percent and 2.9 percent for voltage and current signals, respectively, considering an exact number of switches, thus provide a more valuable solution as compared to [28] and [29]. The results have shown a 71.95% improvement in current THDs and a 13.91% improvement in voltage THDs as compared to the technique presented in [29]. The overall comparison is shown in Table. 4.

We can note from table 4, that the proposed ANN based technique is using more feasible input DC voltage ratios as compared to [29] and is using less number of switching devices as compared to [28] for the production of same number of levels and better THD ratios. It is also worth mentioning that reference model [29] was unable to get better THD ratios in current and voltage ratios even with 27 levels whereas we have achieved the better THD ratios at 15 levels. Hence we can conclude that, the proposed technique is better in terms of performance, losses, efficiency, and overall cost.

D. HARDWARE IMPLEMENTATION

To validate the simulation results, a prototype of the proposed MLI was designed. The solar panels were replaced with 12V DC batteries. And IRF640N MOSFETs were used as power switches, all the diodes were 1N4007 Si diodes. A single-layer PCB was designed with a trace width of 2mm to allow large currents. Arduino UNO was used to provide the PWM. The programming of the UNO was done in C language and the stable Arduino compiler was used to generate and burn the HEX file in the microcontroller. The output waveforms were measured by using a SIGLENT SDS 1052DL+ digital oscil-

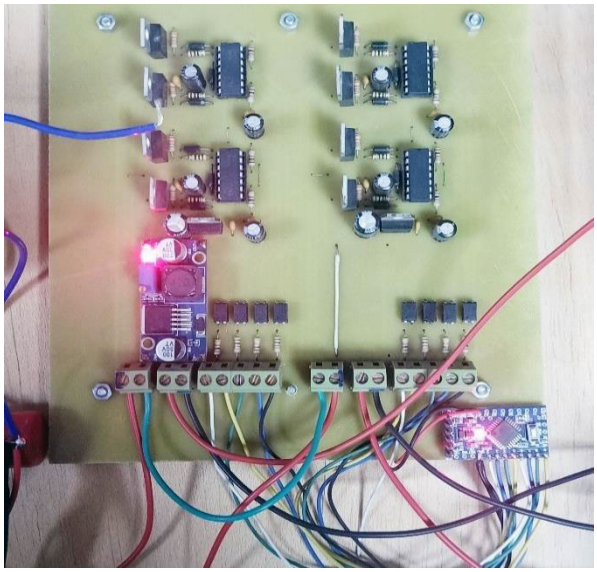

FIGURE 18. Hardware implementation of proposed MLI.

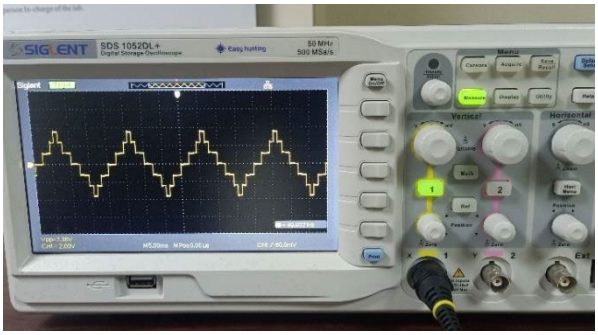

FIGURE 19. 7 voltage levels at 1:2 DC sources.

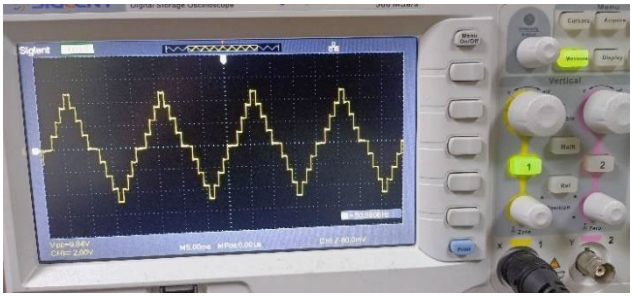

FIGURE 20. 9 voltage levels at 1:3 DC sources.

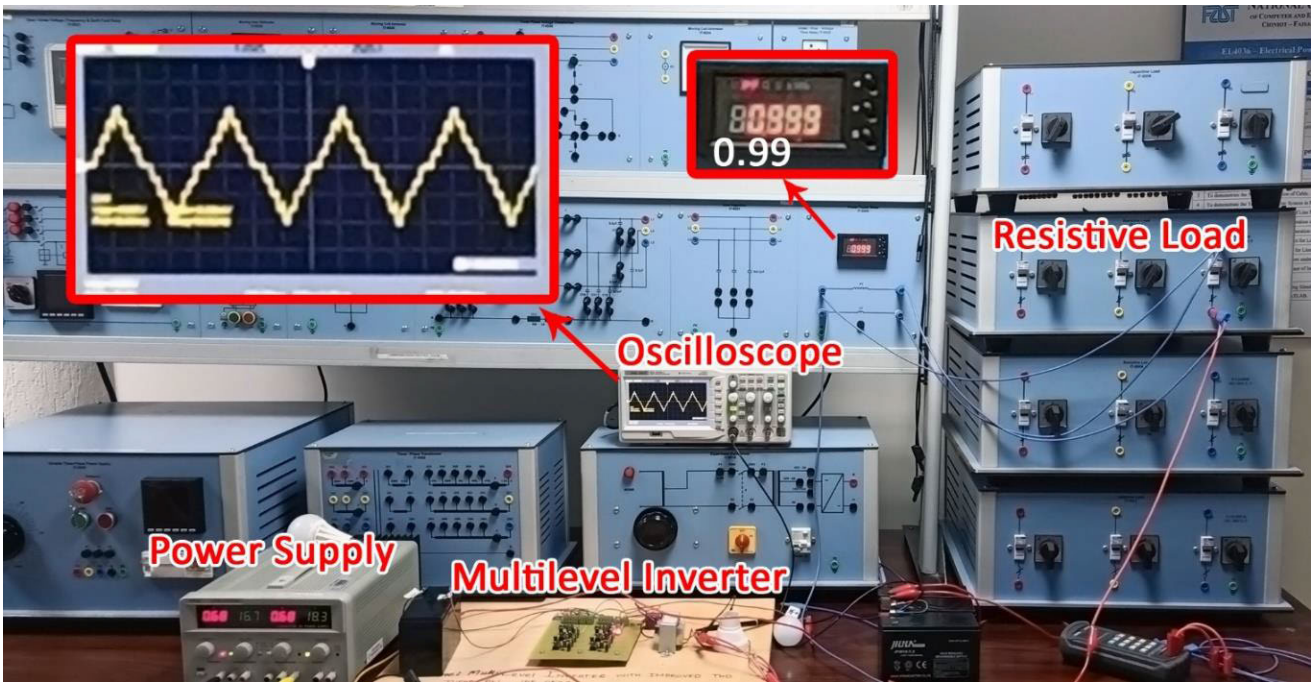

FIGURE 21. Performance of proposed MLI at resistive load.

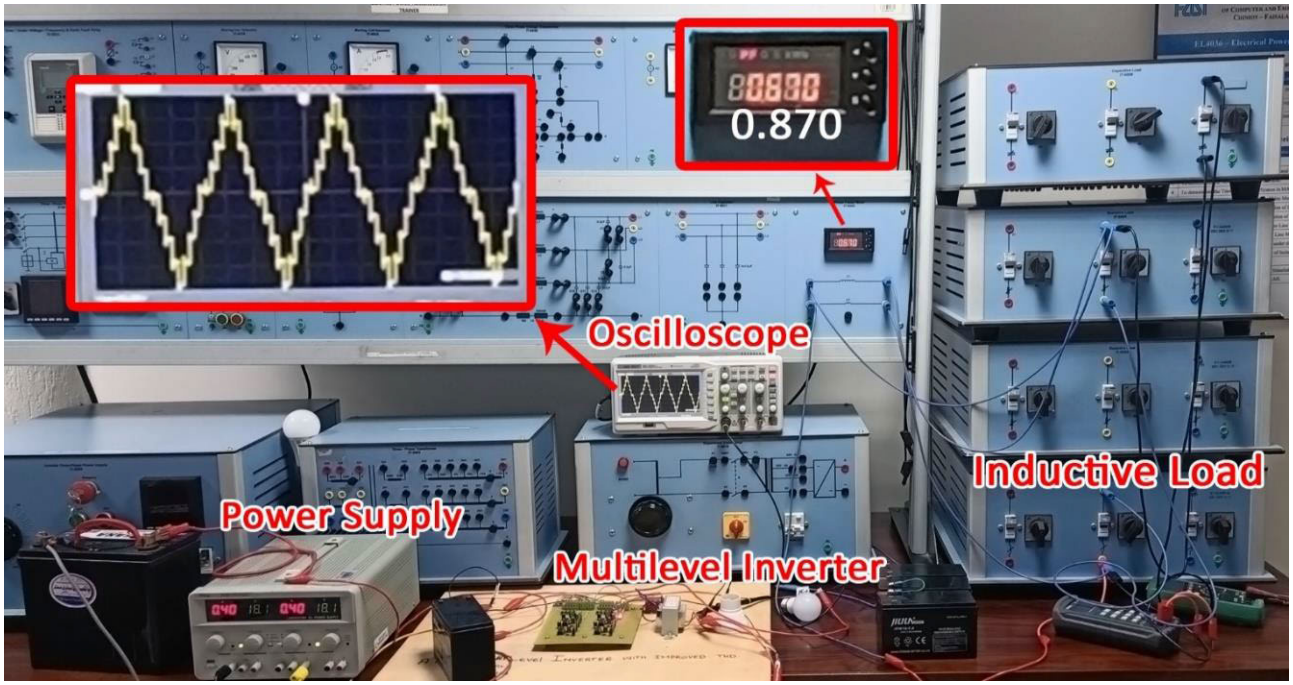

FIGURE 22. Performance of proposed MLI at inductive load.

loscope. The complete hardware setup is shown in figure 18 below.

Due to budget constraints, the experiment was performed by using only 4 batteries, so the circuit was first tested with a DC ratio of 1:2, and the output levels were recorded the obtained 7 levels are shown in Figure 19 below.

Then the circuit was tested with a DC ratio of 1:3 and the output voltage levels were measured the obtained 9 levels are shown in Figure 20.

By using 1:2, the number of levels obtained was 7, and by using 1:3 the number of obtained levels was 9, if we exclude the 0 levels (as it is appearing in both cases), we can conclude

that by using the 1:2:3 ratio we can obtain 15 levels with the proposed configuration.

The designed inverter was then tested on resistive and inductive loads and the output waveform and power factor were recorded by using the state-of-the-art apparatus of a power electronics trainer. The standard resistive and inductive load boxes were used to act as heavy loads. At the resistive load, the power factor of the inverter was measured to be 0.99 and no distortion at the output waveform was observed. The experimental setup and output results are shown in Figure 21.

Similarly, the inverter was tested on inductive load as well. The experimental setup and results are shown in Figure 22. At inductive load, the output waveform remains stable, and very less ripples were observed, but the power factor dropped to 0.870. At a very high inductive load, a power factor of 0.870 is quite good and an indicator of good inverter performance and efficiency.

V. CONCLUSION

In the present era of time, renewable energies are proven to be the savior of humanity. However, their increasing penetration in the utility grid is a highlighted issue and needs to be addressed. Therefore, this paper proposed an asymmetric configuration of the solar-powered fifteen-level cascaded H-bridge MLI with a specific input voltage ratio of 1:2:4. Moreover, this paper used the ANN technique to find the optimal switching states, and then this model is analyzed for the industrial loads. Conclusively, this configuration achieved better efficiency than the reference work and resulted in the THD values of 5.94 percent and 2.9 percent for voltage and current signals, respectively, and an efficiency of 89.6% on an inductive load with the same number of switches, which is a significant improvement in the existing literature.

Currently, due to budget constraints, we could not include the waveform of THDs and the effect of switching angles on the THDs. Hence the future work for this research consists of experimentally validating the simulated THDs at various switching angles and also designing the inverter with a single DC source and deploying this solution into a physical on-grid system.

REFERENCES

[1] A. Rehman, A. Rauf, M. Ahmad, A. A. Chandio, and Z. Deyuan, "The effect of carbon dioxide emission and the consumption of electrical energy, fossil fuel energy, and renewable energy, on economic performance: Evidence from Pakistan," *Environ. Sci. Pollut. Res.*, vol. 26, no. 21, pp. 21760–21773, Jul. 2019, doi: 10.1007/s11356-019-05550-y.

[2] R. Inglesi-Lotz, "The impact of renewable energy consumption to economic growth: A panel data application," *Energy Econ.*, vol. 53, pp. 58–63, Jan. 2016, doi: 10.1016/j.eneco.2015.01.003.

[3] A. Razmjoo, L. G. Kaigutha, M. A. V. Rad, M. Marzband, A. Davarpanah, and M. Denai, "A technical analysis investigating energy sustainability utilizing reliable renewable energy sources to reduce CO_2 emissions in a high potential area," *Renew. Energy*, vol. 164, pp. 46–57, Feb. 2021, doi: 10.1016/j.renene.2020.09.042.

[4] A. Bughneda, M. Salem, A. Richelli, D. Ishak, and S. Alatai, "Review of multilevel inverters for PV energy system applications," *Energies*, vol. 14, no. 6, p. 1585, Mar. 2021, doi: 10.3390/en14061585.

[5] T.-H. Le, Y. Chang, and D. Park, "Renewable and nonrenewable energy consumption, economic growth, and emissions: International evidence," *Energy J.*, vol. 41, no. 2, pp. 73–92, Apr. 2020, doi: 10.5547/01956574.41.2.thle.

[6] S. Chu, Y. Cui, and N. Liu, "The path towards sustainable energy," *Nature Mater.*, vol. 16, no. 1, pp. 16–22, Jan. 2017, doi: 10.1038/nmat4834.

[7] H. E. Gelani, F. Dastgeer, Z. Idrees, K. Amjad, and N. Javed, "Barriers in the progress of domestic biogas plants in rural Pakistan," *Int. J. Sustain. Energy*, vol. 41, no. 6, pp. 713–729, Sep. 2021, doi: 10.1080/14786451.2021.1976179.

[8] U. Yılmaz, Ö. Türksoy, T. İbrikçi, and A. Teke, "Estimation of electrical characteristics and maximum power point of photovoltaic panel," *J. Electr. Syst.*, vol. 13, no. 2, pp. 255–265, 2017.

[9] R. Sekar, D. S. Suresh, and H. Naganagouda, "A review on power electronic converters suitable for renewable energy sources," in *Proc. Int. Conf. Electr., Electron., Commun., Comput., Optim. Techn. (ICEECCOT)*, Dec. 2017, pp. 501–506, doi: 10.1109/ICEECCOT.2017.8284556.

[10] A. Luque and S. Hegedus, Eds., *Handbook of Photovoltaic Science and Engineering: Luque/Photovoltaic Science and Engineering*. Chichester, U.K.: Wiley, 2003, doi: 10.1002/0470014008.

[11] M. Malinowski, K. Gopakumar, J. Rodriguez, and M. A. Pérez, "A survey on cascaded multilevel inverters," *IEEE Trans. Ind. Electron.*, vol. 57, no. 7, pp. 2197–2206, Jul. 2010, doi: 10.1109/TIE.2009.2030767.

[12] E. Babaei, C. Buccella, and M. Saeedifard, "Recent advances in multilevel inverters and their applications—Part I," *IEEE Trans. Ind. Electron.*, vol. 63, no. 11, pp. 7145–7147, Nov. 2016, doi: 10.1109/TIE.2016.2602270.

[13] X. Zhang, T. Zhao, W. Mao, D. Tan, and L. Chang, "Multilevel inverters for grid-connected photovoltaic applications: Examining emerging trends," *IEEE Power Electron. Mag.*, vol. 5, no. 4, pp. 32–41, Dec. 2018, doi: 10.1109/MPEL.2018.2874509.

[14] M. Sarebanzadeh, M. A. Hosseinzadeh, C. Garcia, E. Babaei, S. Islam, and J. Rodriguez, "Reduced switch multilevel inverter topologies for renewable energy sources," *IEEE Access*, vol. 9, pp. 120580–120595, 2021, doi: 10.1109/ACCESS.2021.3105832.

[15] A. Salem, H. Van Khang, I. N. Jiya, and K. G. Robbersmyr, "Hybrid three-phase transformer-based multilevel inverter with reduced component count," *IEEE Access*, vol. 10, pp. 47754–47763, 2022, doi: 10.1109/ACCESS.2022.3171849.

[16] S. Rahman, M. Meraj, A. Iqbal, L. Ben-Brahim, H. Abu-Rub, and I. Khan, "Novel level-shifted PWM technique for cascaded multilevel quasi-impedance source inverter," *IEEE J. Emerg. Sel. Topics Power Electron.*, vol. 9, no. 5, pp. 5918–5928, Oct. 2021, doi: 10.1109/JESTPE.2021.3096844.

[17] S. Sezen and E. Ozdemir, "Modeling, simulation and control of three-phase three level multilevel inverter for grid connected photovoltaic system," *J. Optoelectron. Adv. Mater.*, vol. 15, nos. 3–4, pp. 335–341, Apr. 2013.

[18] R. M. Patil, V. P. Dhote, and A. Thosar, "Comparative analysis of three phase 5,7 9 level inverter using PDPWM technique," in *Proc. Int. Conf. Smart Electr. Drives Power Syst. (ICSEDPS)*, Jun. 2018, pp. 323–328, doi: 10.1109/ICSEDPS.2018.8536031.

[19] G.Vidhya Krishnan, M.Valan Rajkumar, and C.Hemalatha, "Modeling and simulation of 13-level cascaded hybrid multilevel inverter with less number of switches," *Int. J. Innov. Stud. Sci. Eng. Technol.*, vol. 2, no. 11, pp. 43–47, Nov. 2016.

[20] F. Bonanno, G. Capizzi, and G. L. Sciuto, "Solving harmonics reduction problem in multilevel inverters by switching neural networks-based approach," in *Proc. Int. Conf. Clean Electr. Power (ICCEP)*, Taormina, Italy, Jun. 2015, pp. 749–754, doi: 10.1109/ICCEP.2015.7177576.

[21] Kirti Manish Kumar and Vishnu Goyal, "Implementation of algebraic method based selective harmonic elimination of multilevel inverter using artificial neural networks," *Int. J. Electron. Eng. Res.*, vol. 9, no. 4, pp. 467–482, 2017.

[22] K. Yang, J. Hao, and Y. Wang, "Switching angles generation for selective harmonic elimination by using artificial neural networks and quasi-Newton algorithm," in *Proc. IEEE Energy Convers. Congr. Expo. (ECCE)*, Milwaukee, WI, USA, Sep. 2016, pp. 1–5, doi: 10.1109/ECCE.2016.7855483.

[23] W. H. Press, Ed., *Numerical Recipes: The Art of Scientific Computing*, 3rd ed. Cambridge, U.K.: Cambridge Univ. Press, 2007.

[24] A. Basit, S. Khan, A. Wahab, K. Jalal, W. Gohar, and K. Hussain, "The simulation of 3-phase 17-level inverter using two cascaded square wave bridge," *Techinum*, vol. 3, no. 2, pp. 92–108, 2021.

[25] S. Selvaperumal and M. S. S. Sundari, "A comparative analysis of multi-carrier modulation strategies for cascaded H-Bridge multilevel inverter," *J. Comput. Theor. Nanosci.*, vol. 14, no. 12, pp. 6020–6029, Dec. 2017, doi: 10.1166/jctn.2017.7051.
[26] T. Sunitha, K. Udhayakumar, T. Annamalai, and C. Gopinath, "A new 23 level cascaded multi-level inverter with optimum structure," in *Proc. 4th Int. Conf. Electr. Energy Syst. (ICEES)*, Feb. 2018, pp. 320–327, doi: 10.1109/ICEES.2018.8443220.
[27] L. J. Varghese, S. S. Jacob, S. Banumathi, L. Ravi, S. Vairavasundaram, and I. J. Raglend, "Fuzzy based optimal switching angle-PWM controller for 27-level asymmetric multi-level inverter," *J. Intell. Fuzzy Syst.*, vol. 39, no. 6, pp. 8507–8519, Dec. 2020, doi: 10.3233/jifs-189168.
[28] V. Kumar, A. J. Varghese, and R. Roy, "Output voltage regulation techniques improve power quality in solar-fed cascaded multilevel inverters," *J. Eng. Sci.*, vol. 13, no. 6, pp. 593–603, Jun. 2022.
[29] B. Gayathri Devi and B. K. Keshavan, "A novel hybrid phase shifted-modified synchronous optimal pulse width modulation based 27-level inverter for grid-connected PV system," *Energy*, vol. 178, pp. 309–317, Jul. 2019, doi: 10.1016/j.energy.2019.03.173.
[30] H. Khoun-Jahan, A. M. Shotorbani, M. Abapour, K. Zare, S. H. Hosseini, F. Blaabjerg, and Y. Yang, "Switched capacitor based cascaded half-bridge multilevel inverter with voltage boosting feature," *CPSS Trans. Power Electron. Appl.*, vol. 6, no. 1, pp. 63–73, Mar. 2021, doi: 10.24295/CPSSTPEA.2021.00006.
[31] S. S. Lee, B. Chu, N. R. N. Idris, H. H. Goh, and Y. E. Heng, "Switched-battery boost-multilevel inverter with GA optimized SHEPWM for standalone application," *IEEE Trans. Ind. Electron.*, vol. 63, no. 4, pp. 2133–2142, Apr. 2016, doi: 10.1109/TIE.2015.2506626.
[32] U. R. Muthyala and A. Dhabale, "Comparative analysis of switching angle calculation methods for multilevel inverters," *Int. Trans. Elect. Energy Syst.*, vol. 31, no. 8, Aug. 2021, Art. no. e12978, doi: 10.1002/2050-7038.12978.
[33] V. Kachitvichyanukul, "Comparison of three evolutionary algorithms: GA, PSO, and DE," *Ind. Eng. Manage. Syst.*, vol. 11, no. 3, pp. 215–223, Sep. 2012, doi: 10.7232/iems.2012.11.3.215.
[34] S. Arora and B. Barak, *Computational Complexity: A Modern Approach*. Cambridge, U.K.: Cambridge Univ. Press, 2009.
[35] R. Dewani, K. Gopakumar, U. Loganathan, and S. Bhattacharya, "A general multilevel polygonal space vector generation scheme with reduced switching for the inverter and harmonic suppression using a switched-capacitive filter for the full modulation range," *IEEE Trans. Power Electron.*, vol. 37, no. 7, pp. 8167–8176, Jul. 2022, doi: 10.1109/TPEL.2022.3152497.
[36] B. Sah, P. Kumar, and S. K. Bose, "A fuzzy logic and artificial neural network-based intelligent controller for a vehicle-to-grid system," *IEEE Syst. J.*, vol. 15, no. 3, pp. 3301–3311, Sep. 2021, doi: 10.1109/JSYST.2020.3006338.
[37] S. Chavlis and P. Poirazi, "Drawing inspiration from biological dendrites to empower artificial neural networks," *Current Opinion Neurobiol.*, vol. 70, pp. 1–10, Oct. 2021, doi: 10.1016/j.conb.2021.04.007.
[38] O. I. Abiodun, A. Jantan, A. E. Omolara, K. V. Dada, A. M. Umar, O. U. Linus, H. Arshad, A. A. Kazaure, U. Gana, and M. U. Kiru, "Comprehensive review of artificial neural network applications to pattern recognition," *IEEE Access*, vol. 7, pp. 158820–158846, 2019, doi: 10.1109/ACCESS.2019.2945545.
[39] N. Dey, S. Borra, A. Ashour, and F. Shi, Eds., *Machine Learning in Bio-Signal Analysis and Diagnostic Imaging*. London, U.K.: Elsevier, 2019.
[40] K. Muralitharan, R. Sakthivel, and R. Vishnuvarthan, "Neural network based optimization approach for energy demand prediction in smart grid," *Neurocomputing*, vol. 273, pp. 199–208, Jan. 2018, doi: 10.1016/j.neucom.2017.08.017.
[41] E. D. Reyes-Téllez, "Analysis of transfer functions and normalizations in an ANN model that predicts the transport of energy in a parabolic trough solar collector," *Desalin. Water Treat*, vol. 200, pp. 23–41, Oct. 2020, doi: 10.5004/dwt.2020.26063.
[42] S. Hayou, A. Doucet, and J. Rousseau, "On the impact of the activation function on deep neural networks training," 2019, *arXiv:1902.06853*.
[43] G. Mourgias-Alexandris, A. Tsakyridis, N. Passalis, A. Tefas, K. Vyrsokinos, and N. Pleros, "An all-optical neuron with sigmoid activation function," *Opt. Exp.*, vol. 27, no. 7, p. 9620, Apr. 2019, doi: 10.1364/oe.27.009620.
[44] J. Schmidt-Hieber, "Nonparametric regression using deep neural networks with ReLU activation function," *Ann. Statist.*, vol. 48, no. 4, pp. 1875–1897, Aug. 2020, doi: 10.1214/19-aos1875.
[45] I. Kouretas and V. Paliouras, "Simplified hardware implementation of the softmax activation function," in *Proc. 8th Int. Conf. Modern Circuits Syst. Technol. (MOCAST)*, Thessaloniki, Greece, May 2019, pp. 1–4, doi: 10.1109/MOCAST.2019.8741677.
[46] F. B. Grigoletto, "Space vector modulation for three-phase multilevel switched-capacitor inverter," *IEEE Latin Amer. Trans.*, vol. 19, no. 4, pp. 575–583, Apr. 2021, doi: 10.1109/TLA.2021.9448540.
[47] M. T. Islam, H. H. Fayek, E. Rusu, and M. F. Rahman, "A novel hexagonal-shaped multilevel inverter with reduced switches for grid-integrated photovoltaic system," *Sustainability*, vol. 13, no. 21, p. 12018, Oct. 2021, doi: 10.3390/su132112018.
[48] L. Zhang, W. Hong, C. Gao, R. Liu, Q. Yu, and C. Wei, "Selected harmonic mitigation PWM power matching control strategy for asymmetric cascaded H-bridge multilevel inverter," *IEEE J. Emerg. Sel. Topics Power Electron.*, vol. 10, no. 4, pp. 4059–4072, Aug. 2022, doi: 10.1109/JESTPE.2021.3137337.
[49] N. Prabaharan and K. Palanisamy, "Analysis of cascaded H-bridge multilevel inverter configuration with double level circuit," *IET Power Electron.*, vol. 10, no. 9, pp. 1023–1033, Jul. 2017, doi: 10.1049/iet-pel.2016.0506.
[50] M. F. Kangarlu and E. Babaei, "A generalized cascaded multilevel inverter using series connection of submultilevel inverters," *IEEE Trans. Power Electron.*, vol. 28, no. 2, pp. 625–636, Feb. 2013, doi: 10.1109/TPEL.2012.2203339.
[51] J. Ebrahimi, E. Babaei, and G. B. Gharehpetian, "A new multilevel converter topology with reduced number of power electronic components," *IEEE Trans. Ind. Electron.*, vol. 59, no. 2, pp. 655–667, Feb. 2012, doi: 10.1109/TIE.2011.2151813.

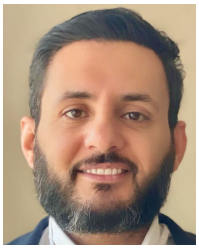

YAZEED YASIN GHADI received the Ph.D. degree in electrical and computer engineering from The University of Queensland. He is currently an Assistant Professor of software engineering with Al Ain University. He was a Postdoctoral Researcher with The University of Queensland, before joining Al Ain University. He has published more than 25 peer-reviewed journals and conference papers and he holds three pending patents. His current research interests include novel electro-acousto-optic neural interfaces for large-scale high-resolution electrophysiology and distributed optogenetic stimulation. He was a recipient of several awards. His dissertation on developing novel hybrid plasmonicphotonic on-chip biochemical sensors received the Sigma Xi Best Ph.D. Thesis Award.

MUHAMMAD SAJID IQBAL received the B.S. degree in telecommunication engineering from NUCES-FAST Karachi, Pakistan, in 2011, and the M.S. degree in electrical engineering from the King Fahd University of Petroleum and Minerals, Saudi Arabia. He is currently a Lecturer with the Electrical Engineering Department, NUCES-FAST Chiniot–Faisalabad. His research interests include power electronic devices, fault-tolerant control for industrial application, antenna array design, and machine learning.

MUHAMMAD ADNAN received the B.S. degree in electrical engineering from the National University of Computer and Emerging Sciences, Peshawar, Pakistan, in 2013, the M.S. degree in electrical engineering from the COMSATS Institute of Information and Technology, Islamabad, Pakistan, in 2015, and the Ph.D. degree in electrical engineering from the National University of Computer and Emerging Sciences. He was a Research Fellow with the Department of Electrical Power Engineering, National University of Computer and Emerging Sciences, from January 2017 to December 2019. He is currently an Assistant Professor with the Department of Electrical Engineering, NUCES-FAST Chiniot–Faisalabad. His research interests include energy management systems, load flow balancing, load forecasting, power systems dynamic analysis, protection, stability, and intelligent control in renewable energy resources using a fuzzy controller and unified power flow controller.

KASHIF AMJAD received the B.S. degree in electrical engineering from the University of Engineering and Technology, Lahore, Lahore, in 2018, and the M.S. degree from the National University of Computer and Emerging Sciences, in 2022. He is currently a Lecturer with the Punjab Group of Colleges. His research interests include microgrid modeling, forecasting, and control and optimization of power systems.

IJAZ AHMAD received the B.S. degree in electrical engineering from the COMSATS Institute of Information and Technology, Abbottabad, Pakistan, in 2017, and the M.S. degree in electrical engineering from the National University of Science and Technology, Islamabad, Pakistan, in 2021. Currently, he is working as a Research Associate (R.A) with the Department of Electrical Engineering in FAST NUCES, CFD Campus. His research interests include energy management systems, load flow balancing, load forecasting, power systems dynamic analysis, protection, stability, and intelligent control in renewable energy resources using a fuzzy controller and unified power flow controller.

UMER FAROOQ received the master's degree in computer engineering from the University of Engineering and Technology, Lahore, Lahore. He is currently a Lecturer with Information Technology University, Pakistan. His research interests include the domain of edge computed embedded systems and applying ML models to electrical systems.